Catalysis Today 166 (2011) 172–179

Contents lists available at ScienceDirect

Catalysis Today

journal homepage: www.elsevier.com/locate/cattod

CO oxidation on gold nanoparticles supported over titanium oxide nanotubes

Mario Méndez-Cruz [a], Jorge Ramírez-Solís [a,b,*], Rodolfo Zanella [c]

[a] UNICAT, Departamento de Ingeniería Química, Facultad de Química, Universidad Nacional Autónoma de México, Cd. Universitaria, México D.F. 04510, Mexico
[b] Instituto Mexicano del Petróleo, Eje Central Lázaro Cárdenas Norte 152, San Bartolo Atepehuacan, México D.F. 07730, Mexico
[c] Centro de Ciencias Aplicadas y Desarrollo Tecnológico, Universidad Nacional Autónoma de México, Cd. Universitaria, México D.F. 04510, Mexico

ARTICLE INFO

Article history:
Available online 31 July 2010

Keywords:
Titanium oxide nanotubes
CO oxidation
Deposition–precipitation
Gold

ABSTRACT

Titanium oxide nanotubes (TN) were synthesized and used as support for Au nanoparticles obtained by deposition–precipitation with urea. The activity of Au/TN catalysts prepared under different conditions was tested in the oxidation of CO. The results indicate that titanium oxide nanotubes (TN) can be used as support for gold nanoparticles obtained by deposition–precipitation, since adequate gold nanoparticle sizes (<5 nm.) for CO oxidation can be obtained.

Varying the preparation conditions of the catalysts it was found that the best catalyst performance is obtained by calcining the TN support at temperatures higher than 400 °C, temperature at which the trititanate phase obtained in the as-prepared material is completely transformed into TiO_2-anatase. Higher calcination temperatures lead to a significant decrease in the surface area of TN.

It was also observed that the activity of the Au/TN catalysts was negatively affected by long storage periods. This fact was evidenced by the significant increase in gold particle size, which is apparently due to the high mobility of gold nanoparticles on the support.

Increasing the gold loading from 3 to 9 wt% does not improve the CO oxidation activity because, at 9 wt% Au the particle sintering increases leading to particles greater than 5 nm, which are not effective for CO oxidation.

To obtain good catalytic activity it is necessary to pretreat the catalysts at least at 300 °C to assure the complete reduction of the gold precursor. The use of hydrogen or air in the catalyst pretreatment to obtain the reduction of the gold precursor did not affect the performance catalysts.

1. Introduction

Titanium oxide nanotubes (TN) prepared by hydrothermal synthesis have attracted special attention since 1998, when Kasuga published his work describing them for the first time [1]; since then some researchers have published works related to their synthesis [2–19,28] or applications [20–27]. TN present three main advantages: high specific area (400 m^2/g) [1], low cost, and feasibility to be produced in great quantities. These materials can be potentially used in the fields of photocatalysis [20,29,31], solar cells [21], adsorbents [22] and heterogeneous catalysis [23–28,30,32,33]. Specifically, TN have been used as catalytic support for different metal active phases (metallic, oxides or sulfides): platinum for cyclohexene hydrogenation–dehydrogenation [23], copper for NO reduction with NH_3 [24], cobalt and molybdenum for fuels hydrodesulfurization (HDS) [25–27], iridium and cobalt for water splitting for hydrogen production [28], iron for photocatalytic oxidation of acetaldehyde [29], gold for water–gas shift reaction [30], photocatalytic mineralization of benzene [31] and CO oxidation [32,33].

Gold is a metal with no reactivity in bulk, but if it is divided into nanoparticles it displays high activity for several reactions; Haruta et al. showed that gold nanoparticles supported on oxides can perform the carbon monoxide (CO) oxidation [35]. This application is interesting for pollution control because of the capability of gold nanoparticles to oxidize CO at temperatures even lower than 0 °C. It has been shown that the reactivity of gold depends on both the nanoparticle size, which must be lower than 5 nm [36], and on the support used. Titanium oxide has demonstrated to be one of the best supports [36,37], despite its low specific area (45 m^2/g) as in Degussa P-25 [38]. A way to improve the Au/TiO_2 catalysts would be the use of TiO_2 supports with high specific surface area. It appears interesting then to analyze the performance of Au nanoparticles supported on TiO_2 nanotubes in the CO oxidation reaction, and test their activity and stability when some of the preparation and catalyst activation conditions are varied.

An adequate way to support gold nanoparticles on TiO_2 with sizes below 5 nm is the deposition–precipitation method used by

* Corresponding author at: UNICAT, Departamento de Ingeniería Química, Facultad de Química, Universidad Nacional Autónoma de México, Cd. Universitaria, México D.F. 04510, Mexico. Tel.: +52 55 56225349; fax: +52 55 56225366.
E-mail address: jrs@unam.mx (J. Ramírez-Solís).

0920-5861/$ – see front matter © 2010 Elsevier B.V. All rights reserved.
doi:10.1016/j.cattod.2010.06.014

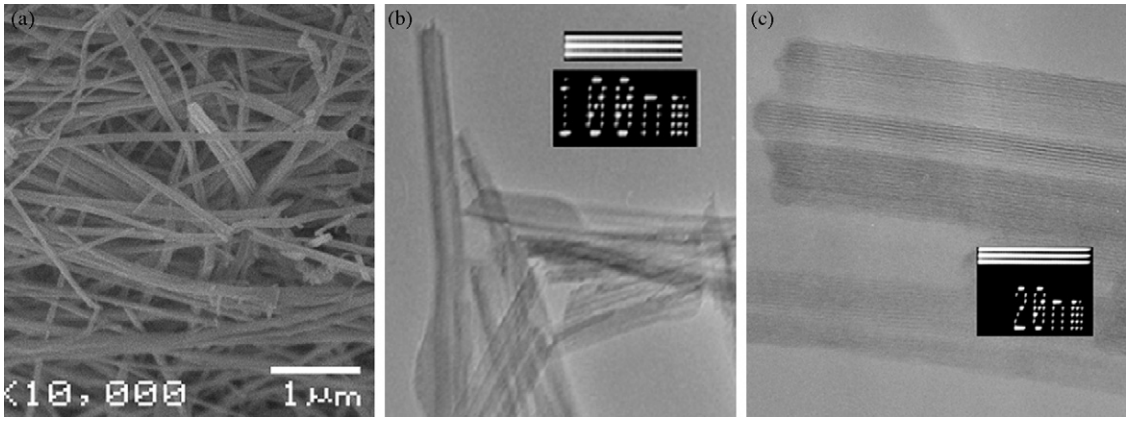

Fig. 1. (a) SEM image of as-prepared TN; (b) TEM image of as-prepared TN; and (c) magnified TEM image of a nanotube, where a central channel and wall details can be observed.

Zanella et al. [38–40], which uses urea to increase the solution pH instead of sodium hydroxide as proposed by Haruta et al. [35]. The aforementioned method allows the deposition of metal loadings close to 100% of the metal in solution.

In the present work we analyze the possibility to obtain highly active CO oxidation catalysts by the deposition of gold nanoparticles, smaller than 5 nm, over titanium oxide nanotubes (TN). In particular, attention will be focused on the changes produced in the CO oxidation activity when the calcination temperature of the support, the storing time of catalysts, the gold loading and thermal treatment conditions before reaction (temperature and gas type) are varied. To this end the supports and catalysts were characterized by N_2 fisisorption, X-ray diffraction and transmission electron microscopy (TEM). The catalysts were evaluated in the CO oxidation reaction using a temperature-programmed reaction system.

2. Experimental

2.1. Support preparation

Titanium oxide nanotubes (TN) were prepared as described elsewhere according to Kasuga's method [1]. In short, 2 g of TiO_2 (P-25, Degussa) were mixed with 134 mL of an aqueous solution of NaOH (10 M). The mixture was kept under stirring in a Teflon autoclave at 110 °C for 24 h. Then, the autoclave was quickly cooled to room temperature and opened to recover a white precipitate, which was thoroughly washed with distilled water and with an aqueous solution of HCl (0.1 M). The product was then filtered, dried in air at 120 °C for 12 h and later calcined in static air at 300–500 °C for 4 h.

2.2. Au/TN preparation

One gram of TN was suspended in 37 mL of an aqueous solution of $HAuCl_4{\cdot}3H_2O$ (0.0042 M) and urea (0.42 M) at room temperature in a vessel protected from light. Then the suspension was heated up to 80 °C and kept under stirring for 16 h to allow the deposition–precipitation of gold over the support surface, then the mixture was centrifuged to recover the solid. To eliminate residual ions, the solid was stirred in 50 mL of distilled water at 50 °C and centrifuged again at 50 °C, this process was repeated four times. The solid was then dried under vacuum at 80 °C for 2 h and stored away from light in a desiccator under vacuum at room temperature. The same procedure was applied to prepare a Au/TiO_2 catalyst but in this case the support employed was titania P-25 (Degussa). Catalysts with 3 and 9 wt% Au were prepared. The catalyst with high Au load was only used for the experiments performed to analyze the effect of gold load.

2.3. Characterizations

SEM images and EDX microanalysis were obtained using a JEOL JSM-5900 LV scanning electron microscope equipped with an Oxford-Isis energy dispersive X-ray analyzer. TEM images were obtained using a JEOL 2010 transmission electron microscope at 200 kV. For TEM analysis the samples were dispersed by ultrasonication in ethyl alcohol for 20 min and a drop of the supernatant liquid was placed onto a holey carbon film supported on a copper grid. The structure of the nanotubes was characterized by X-ray diffraction (XRD) using a Siemens D5000 diffractometer with a Cu Kα source (λ = 1.5406 Å). Textural properties were determined by nitrogen physisorption, using a Micromeritics TriStar apparatus. The specific area was calculated from Brunauer–Emmett–Teller (BET) equation and the pore size distribution was analyzed with the Barrett–Joyner–Halenda (BJH) method. The catalytic experiments were performed in a In Situ Research RIG-150 catalyst characterization system, using a fixed bed quartz reactor with 42.5 mg of catalyst and gas flow of 100 mL/min. The gas mixture consisted of 98% of N_2, 1% of CO and 1% of O_2. The exit gases were analyzed with an online gas chromatograph (Agilent Technologies 6890N) equipped with FID detector and a HP Plot Q column. The temperature during the reaction tests was programmed from −5 to 300 °C with a linear ramp of 2 °C/min. Before the reaction the catalyst was pretreated for 2 h with air or hydrogen (80 mL/min) at temperatures between 200 and 400 °C.

3. Results and discussion

3.1. Nanotube synthesis

SEM observations of the as-prepared material showed the presence of bundles of filaments of different widths, 40–100 nm, and lengths of several hundreds of nanometers (Fig. 1a). The presence of nanotubes was made evident by the observation of the samples by TEM. Fig. 1b and c shows some details of the tubular structure of the filaments. The nanotube walls seem to be formed by several layers separated by ca. 0.7 nm, in good agreement with previous reports of 0.78 and 0.71 nm in the separation of the layers forming the nanotube wall [2,5]. The inner diameter of the observed TN ranged from 5 to 15 nm, and the outer diameter from 11 to 18 nm.

Since the TN are intended to be used as catalyst supports, it is important to know the textural and structural changes that they undergo with the calcination temperature. Fig. 2 shows the TEM images of TN calcined in static air at 300 and 500 °C. It is evident that as the calcination temperature is increased, the tubular structure of the TN, which was well defined for the as-prepared material,

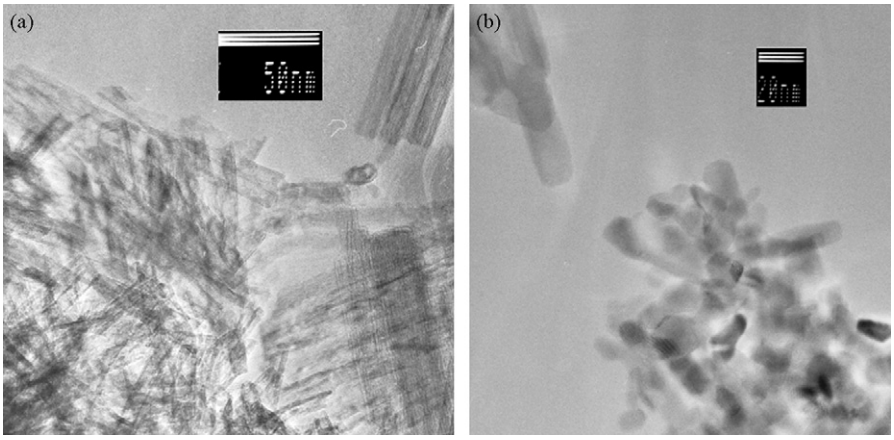

Fig. 2. TEM images of TN calcined in static air for 4 h at: (a) 300 °C and (b) 500 °C.

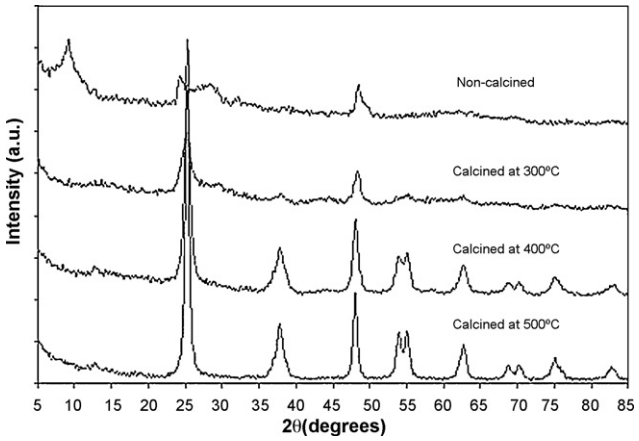

Fig. 3. XRD diffractogram of TN as-prepared and calcined in static air at different temperatures.

becomes less defined at 300 °C and clearly deteriorated at 500 °C. In fact at 500 °C the formation of some round anatase particles of about 20 nm is clearly evident.

The chemical structure of the TN also changes with the calcination temperature. Fig. 3 shows the XRD diffractograms of these materials. Initially, the diffractogram corresponding to the uncalcined nanotubes presents peaks at $2\theta = 9.54$, 24.40, 26.98, 32.28, 48.40 and 50.02, which have been previously assigned to trititanate or trititanic acid ($H_2Ti_3O_7$) in tubular form [2,17]. These peaks diminish their intensity when the material is calcined at 300 °C, while the main peak corresponding to titanium oxide-anatase at $2\theta = 25.34^\circ$ begins to appear. At calcination temperature of 400 °C the trititanate peaks disappear and instead the peaks corresponding to anatase are clearly displayed. Calcination at 500 °C only increases the crystallization of the anatase phase.

The textural properties of the material also reflect the structural and morphological changes observed by TEM and XRD. Fig. 4a shows the N_2 adsorption–desorption isotherms of TN calcined at different temperatures. The isotherms have a shape similar to that reported by Idakiev for titanium oxide nanotubes [30]. As the calcination temperature is increased, the isotherm retains its shape although the amount of nitrogen adsorbed decreases indicating a reduction in pore volume. Indeed, Table 1 shows that as the calcination temperature is increased the pore volume decreases and the average pore diameter increases. Table 1 also shows how the specific area decreases in the uncalcined TN from 318 m^2/g to 296, 155 and 104 m^2/g as the calcination temperature is fixed at 300, 400 and 500 °C, respectively. Looking at the pore size distribution, calculated from the BJH equation in the desorption branch, the peak maximum concerning the pore size of the uncalcined material appears at 16 nm, and increases to 18, 21 and 22 nm when the material is calcined at 300, 400 and 500 °C, respectively (Table 1 and Fig. 4b).

Changes in pore size are probably caused by variations in the size of interlayer spacing of nanotube walls with temperature; Suzuki and Yoshikawa [34] observed that interlayer spacing changed from 9.2 to 7.9 Å when nanotubes were heated from room temperature to 200 °C. In Fig. 3 one peak at 9.2° is observed for the uncalcined nanotubes. This peak corresponds to the interlayer spacing in nanotube walls in contrast, there is no peak corresponding to this feature in calcined nanotubes. This information indicates that the interlayer spacing changes from 9.6 to <2 Å when the nanotubes are heated from room temperature to 300 °C. Interlayer spacing reduction is probably caused by the loss of interlayer water [34], the effect of reducing the interlayer spacing in a spiral is an increase in the inner diameter. The decrease of specific area with calcination is caused by two reasons: the elimination of interlayer spacing in the nanotube walls and transformation of trititanic acid into anatase. As mentioned above, the nanotubes change their structure with calcination, and anatase presents a lower specific area.

3.2. Gold catalysts supported on TN

Table 2 summarizes the support calcination temperatures, gold load, storing time before reaction, and pretreatment conditions (temperature and type of gas) for the AuTN catalysts used in the experimental tests. Samples are named AuTN-01, AuTN-02, etc. The TN were calcined at three different temperatures in static air during 4 h, and later were decorated with gold nanoparticles using the method of deposition–precipitation with urea. To corroborate that gold nanoparticles did not sinter to large sizes during reaction, the TEM images used to evaluate the gold particle size distribution and to observe the nanotubes structure were taken from catalyst samples after reaction. Fig. 5a shows a TEM image of the AuTN-01 catalyst after reaction where gold nanoparticles with average size of 3.2 nm are observed. It is well known that good catalytic activity for CO oxidation is obtained from gold nanoparticles smaller than 5 nm [36]. The TEM micrographs also showed that the tubular structure of nanotube was preserved after reaction.

3.2.1. Effect of calcination temperature of the support (TN) on CO oxidation activity

Fig. 6 shows the plots of CO conversion with reaction temperature for Au/TN catalysts prepared with supports calcined at 300, 400 and 500 °C (samples AuTN-01, AuTN-02 and AuTN-03). The cat-

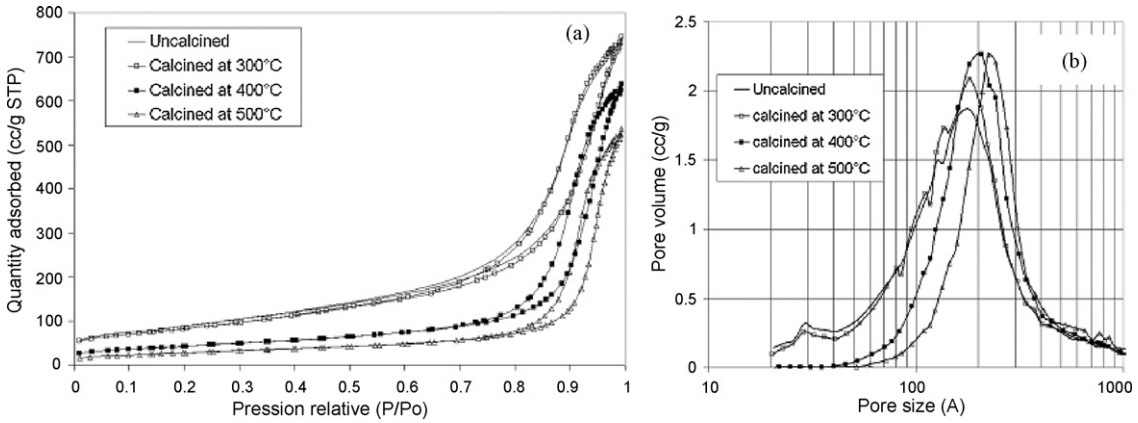

Fig. 4. (a) Adsorption isotherms of TN uncalcined and calcined in static air for 4 h at different temperatures. (b) Pore size distribution of TN obtained from the desorption branch of the corresponding isotherm using the BJH equation.

Table 1
Textural properties of TN as-prepared and calcined at different temperatures.

Sample	Specific surface area (m^2/g)	Pore volume (cm^3/g)[a]	Average pore size (Å)[b]	Pore size at maximum (Å)[c]
TN before calcination	318	1.14	110	116
TN calcined at 300 °C	296	1.16	118	181
TN calcined at 400 °C	155	0.99	186	207
TN calcined at 500 °C	104	0.83	225	224

[a] BJH desorption cumulative volume of pores between 17.000 Å and 3000.000 Å diameter.
[b] BJH desorption average pore diameter (4 V/A).
[c] Taken from Fig. 4b.

Table 2
Catalysts prepared at different synthesis and pretreatment conditions.

Sample	Support calcination temperature (°C)	Wt% Au	Storing time (months)	Pretreatment temperature (°C)	Pretreatment gas
AuTN-01	300	3	1	300	Air
AuTN-02	400	3	1	300	Air
AuTN-03	500	3	1	300	Air
AuTN-04	300	3	12	300	Air
AuTN-05	400	9	1	300	Air
AuTN-06	400	3	1	200	Air
AuTN-07	400	3	1	400	Air
AuTN-08	400	3	1	300	Hydrogen

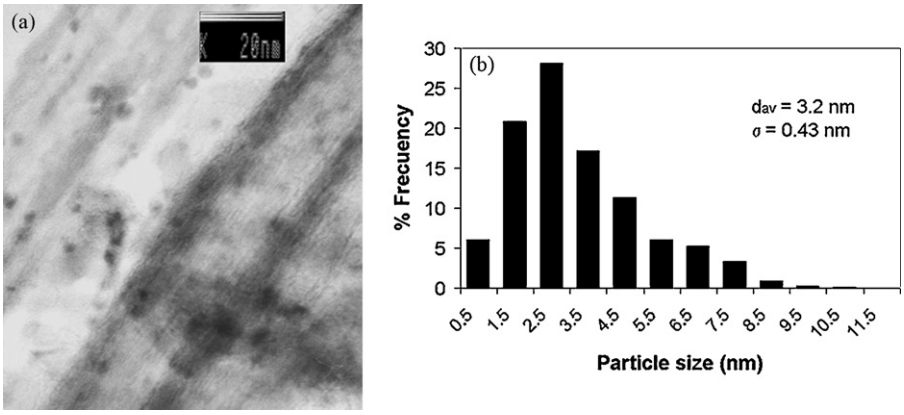

Fig. 5. (a) TEM image of TN decorated with gold nanoparticles. (b) Histogram of gold particles size obtained of the TEM image. d_{av}: average size; σ: standard deviation.

alyst AuTN-01 displayed low activity compared with AuTN-02 and AuTN-03. In fact, these catalysts where the support was calcined at 400 and 500 °C displayed nearly the same activity reaching 100% conversion at about 200 °C. In order to compare activity of the AuTN catalysts with a reference, a catalyst with 3 wt% Au over titania (Degussa P-25) was prepared.

Fig. 6 shows that this catalyst is slightly more active than Au over nanotubes at low temperatures but at 100 °C and beyond its activity is lower than AuTN-02 and AuTN-03.

TEM images of AuTN catalysts (Fig. 7) show that the sizes of gold nanoparticles are in good agreement with the observed activity of the catalysts since AuTN-01 having an average gold particle size of

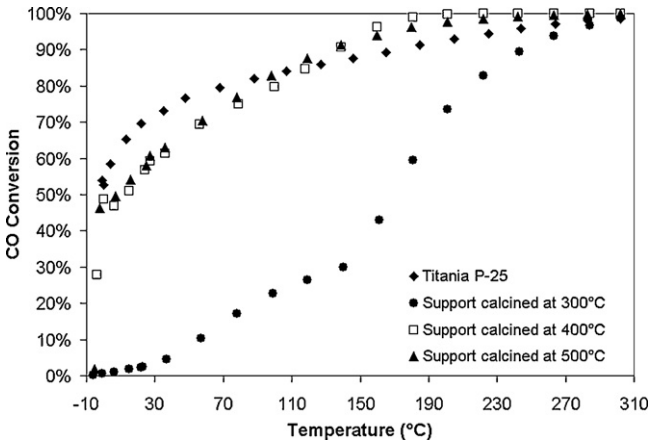

Fig. 6. Activity of Au/TN catalysts (3 wt% Au) over supports calcined at different temperatures and Au/titania (P-25) for CO oxidation.

4.39 nm (Fig. 7a), was the least less active catalyst. On the other hand, AuTN-02 and AuTN-03 show average gold particle sizes of 2.26 (Fig. 7b) and 2.42 nm (Fig. 7c), respectively. These two catalysts display almost the same activity although AuTN-02 is slightly more active, which is in agreement with its smaller gold average particle size. In any case, it seems that the decrease in the particle size below 2.42 nm has little effect on the catalytic activity.

The changes observed in the catalytic activity can be rationalized by observing the structural changes in the supports with calcination temperature, as observed by X-ray diffraction. As Fig. 3 shows, calcination of the support at 300 °C only produced the partial transformation of trititanic acid to anatase, while the calcination at 400 or 500 °C led to the disappearance of the reflections associated with trititanic acid and only peaks corresponding to the anatase phase are observed with crystallization increasing at 500 °C. It seems, then, that Au/trititanic acid catalysts are much less active than the Au/anatase. TEM images (Fig. 7) obtained after reaction indicated that the tubular shape of the support was present in AuTN-01 and AuTN-02, and slightly present in AuTN-03. So, it seems that although the catalytic activity might be related to the support shape, the chemical structure of the support has a more important impact on the catalyst activity.

3.2.2. *Effect of storing time of catalysts*

Zanella et al. [40] noted that gold nanoparticles supported on titania (P-25 Degussa) increase their average size when stored for long periods of time. Clearly this behavior has a detrimental effect on catalytic activity. In our case, Fig. 8 shows the activity evolution for the catalysts belonging to the same preparation batch but stored different times (up to 11 months difference). As it can be observed, there is a decrease in catalytic activity between the catalyst stored 1 month (AuTN-01, average particle size 3.2 nm, Fig. 5b) and the one stored for 12 months (AuTN-04, average particle size 7.84 nm, Fig. 9). The increase in the particle size is probably due to the fact that metallic gold, being a noble metal is not strongly bonded to the support, but by van der Waals interactions and therefore possesses high mobility on the surface, facilitating its sintering.

3.2.3. *Effect of gold loading*

The activity of Au/TN catalysts with two different gold loadings (3 and 9 wt% Au, samples AuTN-02 and AuTN-05, respectively) is compared in Fig. 10. The activity displayed by both catalysts is similar, although the catalyst AuTN-05 is slightly more active.

The cause of this phenomenon can be inferred from the analysis of the particle size histograms obtained from TEM images of the catalysts. A high density of gold nanoparticles is observed in AuTN-05,

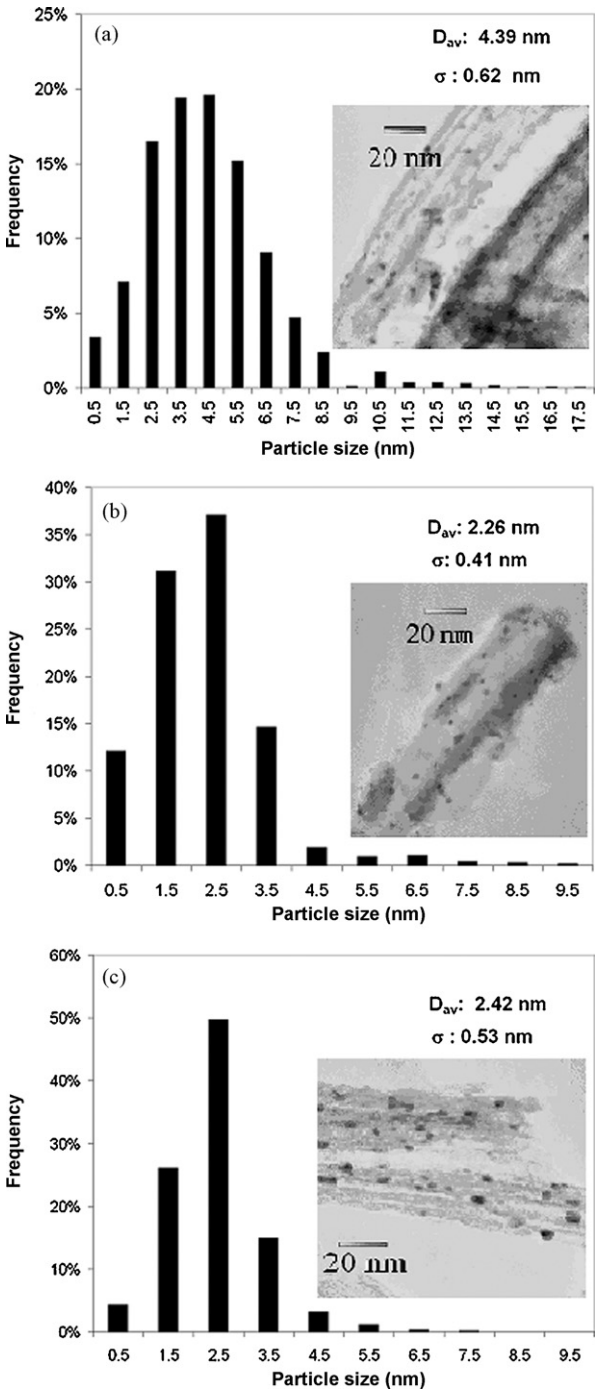

Fig. 7. Particle size histograms for Au/TN catalysts at different calcination temperatures of support: (a) 300 °C; (b) 400 °C; and (c) 500 °C. Pretreatment temperature of the catalysts before reaction: 300 °C. d_{av}: average size; σ: standard deviation.

while the catalyst AuTN-02 had a good dispersion of nanoparticles (Fig. 7b). The high density of nanoparticles causes sinterization, which produce bigger particles, expanding the distribution of particle size (Fig. 11), increasing average gold particle size from 2.26 to 4.23 nm. Gold activity decreases if nanoparticles size increases, but in the case of catalyst AuTN-05 the activity was compensated by the increased amount of particles formed from a higher gold load (3 wt% vs 9 wt%).

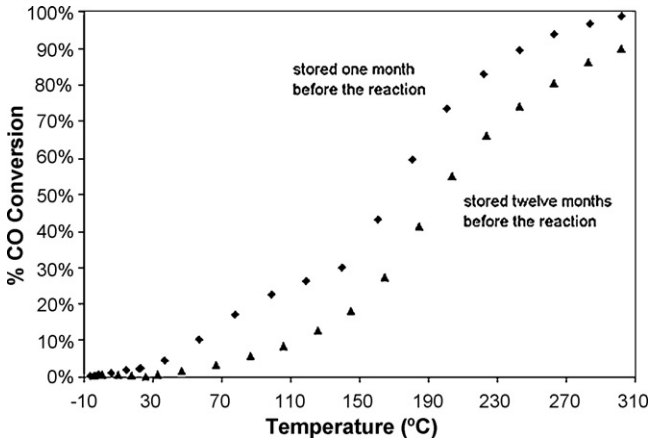

Fig. 8. Activity of Au/TN catalysts (3 wt% metallic gold) for CO oxidation with different storing time. Calcination temperature of support: 300 °C; pretreatment temperature: 300 °C.

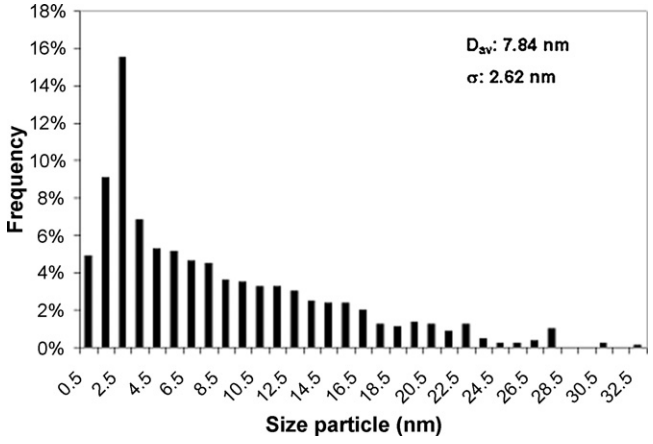

Fig. 9. Histogram of particle size of Au/TN catalyst stored for 12 months. d_{av}: average size; σ: standard deviation.

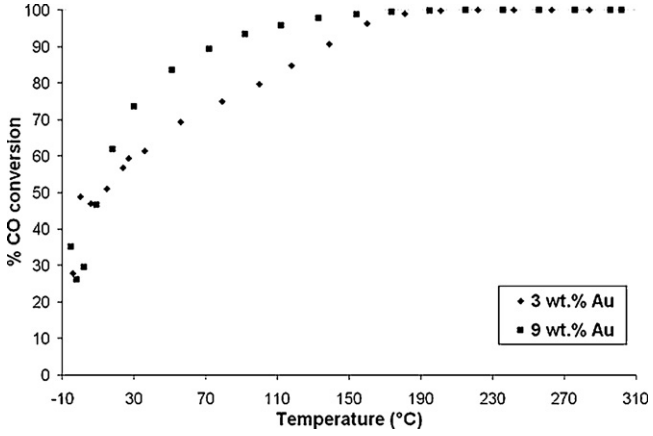

Fig. 10. Activity of Au/TN catalysts for CO oxidation with different gold loads. Calcination temperature of support: 400 °C. Pretreatment temperature: 300 °C.

3.2.4. Effect of pretreatment temperature of catalyst

Another variable to consider is the temperature at which catalyst is pretreated prior to reaction. With this process, the gold precursor is reduced to obtain metallic gold ready for reaction. Fig. 12 shows the activity of the catalysts pretreated at three different temperatures. The catalyst pretreated at 200 °C (sample AuTN-06) shows very low activity, while the catalysts pretreated at

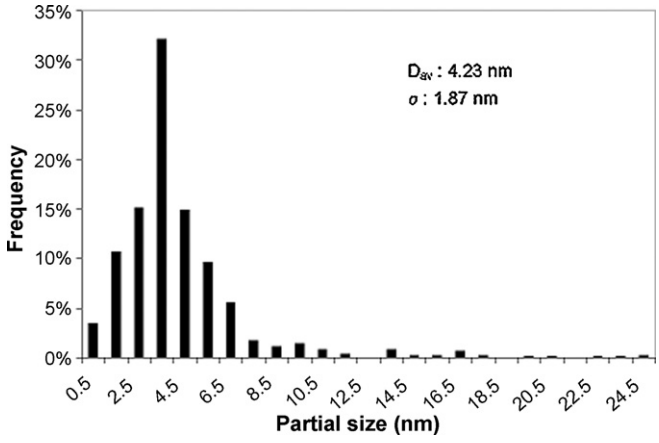

Fig. 11. Histogram of particle size of Au/TN catalyst with 9 wt% of metallic gold. Calcination temperature of support: 400 °C. Pretreatment temperature: 400 °C. d_{av}: average size; σ: standard deviation.

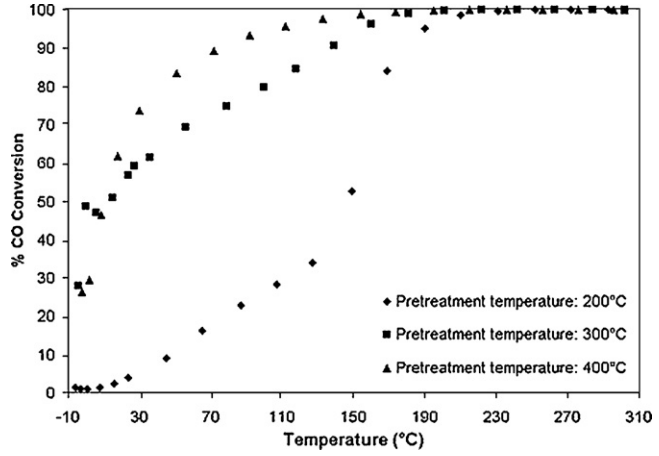

Fig. 12. Activity of Au/TN catalysts (3 wt% of gold) for CO oxidation at different pretreatment temperatures. Calcination temperature of support: 400 °C; pretreatment gas: air.

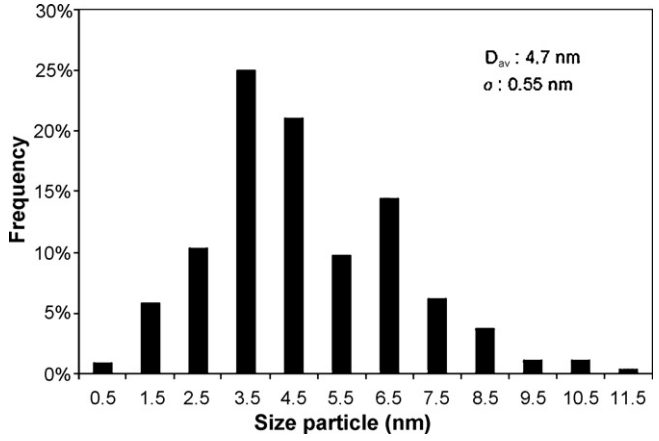

Fig. 13. Histogram of particle size of Au/TN catalyst (3 wt% of Au) pretreated at 200 °C. d_{av}: average size; σ: standard deviation.

300°C (sample AuTN-02) and 400 °C (sample AuTN-07) have high activity, being the last one the more active. These differences in activity could be ascribed to differences either in the dispersion of the particles or in the reduction extent of the gold precursor.

A comparison of the particle size distribution of the AuTN-06 (Fig. 13) with AuTN-02 (Fig. 7b) shows similar gold particle size

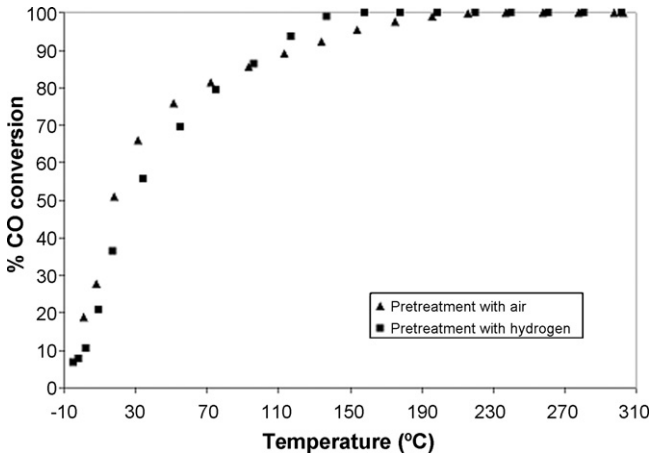

Fig. 14. Activity for CO oxidation of Au/TN catalysts (9 wt% of metallic Au) pretreated with different gases. Pretreatment temperature: 300 °C; calcination temperature of supports: 400 °C.

distribution and practically equal average sizes (4.4 nm vs 4.7 nm). These results indicate that the observed difference in activity is not associated with the dispersion of the gold particles on the support but rather to differences in the reduction extent of the catalyst AuTN-06 respect to AuTN-02. In other words, the gold precursor supported on TN is not completely reduced at 200 °C, and therefore to achieve high activity it is necessary to pretreat the catalyst in air at least at 300 °C. It was previously reported that gold nanoparticles supported over titania (P-25, Degussa) are reduced at 200 °C [39]. It appears then that when supported on TN they require a higher reduction temperature and that this difference is probably associated to the different nature of the supports.

3.2.5. *Effect of pretreatment gas*

To analyze the importance of the nature of the gas used in the pretreatment of the catalyst, the activity of catalysts pretreated with air or hydrogen was compared. It is known that the precursor precipitated using the deposition–precipitation with urea method produces Au^{3+} species [40] that can be reduced in air to Au° in two steps: first the precursor is oxidized into Au_2O_3 and then this oxide reduces to Au°, because it possesses a positive ΔHf (+19.3 kJ/mol), which allows reduction to take place at temperatures above 100 °C [41,42]. When pretreatment takes place with hydrogen, the gold precursor is directly reduced from Au^{3+} to Au°.

Fig. 14 shows the activity of Au/TN catalysts pretreated with air (AuTN-02) or hydrogen (AuTN-08). As it can be observed, the activity of the Au/TN catalysts do not vary with the pretreatment gas (air or hydrogen), indicating that neither the reduction extent nor the particle dispersion are greatly affected by the nature of the reducing gas (hydrogen or air).

4. Conclusions

Nanoparticles of <5 nm can be deposited over titanium oxide nanotubes when urea is used to increase the pH during the deposition–precipitation of gold.

Au/TN catalysts display high activity in the CO oxidation reaction. At reaction temperatures above 120 °C their activity is higher than displayed by Au nanoparticles deposited on TiO2 (P-25 Degussa)

Varying the preparation conditions of Au/TN catalysts it was found the following:

(a) The best catalytic performance was obtained when the TN support was calcined at temperatures of 400 and 500 °C, temperatures at which the trititanic acid obtained during the TN synthesis is completely transformed into TiO_2-anatase.
(b) To obtain high activity in the CO oxidation reaction it is necessary to pretreat the Au/TN catalyst at least at 300 °C to assure the complete reduction of the gold precursor.
(c) The use of hydrogen or air in the pretreatment of the catalyst does not affect its performance in the CO oxidation reaction.
(d) Long periods (12 months) of catalyst storage negatively affect the activity of Au/TN catalysts because they produce significant increases in gold particle size due to the high mobility of the gold nanoparticles on the support.
(e) Increasing the gold load from 3 to 9 wt% Au did not cause an important improvement in the CO oxidation activity of AuTN catalysts because gold particles larger than 5 nm, which are not effective for CO oxidation, are obtained.

Acknowledgements

The authors thank Iván Puente-Lee and Cecilia Salcedo-Luna for technical assistance with HRTEM and powder XRD characterizations, respectively. Mario Méndez Cruz is indebted to CONACYT (México) for Ph.D. grant (CONACYT register no. 183293). Rodolfo Zanella acknowledges PUNTA (IMPULSA 01) and CONACYT 55154 project for the financial support. Jorge Ramírez thanks CONACyT for sabbatical grant (2009) and DGAPA-UNAM for sabbatical grant (2010).

References

[1] T. Kasuga, M. Hiramatsu, A. Hoson, T. Sekino, K. Niihara, Formation of titanium oxide nanotube, Langmuir 14 (1998) 3160–3163.
[2] Q. Chen, G.H. Du, S. Zhang, L.-M. Peng, The structure of trititanate nanotubes, Acta Crystallogr. Sect. B: Struct. Sci. 58 (2002) 587–593.
[3] Y. Zhu, H. Li, Y. Kotylpin, Y. Hacohen, A. Gedanken, Sonochemical synthesis of titania whiskers and nanotubes, Chem. Commun. (2001) 2616–2617.
[4] Q. Zhang, L. Gao, J. Sun, S. Zheng, Preparation of long TiO_2 nanotubes from ultrafine rutile nanocrystals, Chem. Lett. (2002) 226–227.
[5] Y. Wang, G. Hu, X. Duan, H. Sun, Q. Xue, Microstructure and formation mechanism of titanium dioxide nanotubes, Chem. Phys. Lett. 365 (2002) 427–431.
[6] R. Ma, Y. Bando, T. Sasaki, Nanotubes of lepidocrocite titanates, Chem. Phys. Lett. 380 (2003) 577–582.
[7] Y. Chen, C. Lee, M. Yeng, H. Chiu, Preparing titanium oxide with various morphologies, Mater. Chem. Phys. 81 (2003) 39–44.
[8] Z.Y. Yuan, B.L. Su, Titanium oxide nanotubes, nanofibers and nanowires, Colloids Surf. A 241 (2004) 173–183.
[9] W. Wang, O. Varghese, M. Paulose, C. Grimes, A study on the growth and structure of titania nanotubes, J. Mater. Res. 19 (2004) 417–422.
[10] B. Yao, Y. Chan, X. Zhang, W. Zhang, Z. Yang, N. Wang, Formation mechanism of TiO_2 nanotubes, Appl. Phys. Lett. 82 (2003) 281–283.
[11] B. Poudel, W. Wang, C. Dames, J. Huang, S. Kunwar, D. Wang, D. Banerjee, G. Chen, Z. Ren, Formation of crystallized titania nanotubes and their transformation into nanowires, Nanotechnology 16 (2005) 1935–1940.
[12] S. Zhang, L. Peng, Q. Chen, G. Du, G. Dawson, W. Zhou, Formation mechanism of $H_2Ti_3O_7$ nanotubes, Phys. Rev. Lett. 91 (2003) 256103.
[13] R. Ma, K. Fukuda, T. Sasaki, M. Osada, Y. Bando, Structural features of titanate nanotubes/nanobelts revealed by Raman, X-ray absorption fine structure and electron diffraction characterizations, J. Phys. Chem. B 109 (2005) 6210–6214.
[14] A. Nakahira, W. Kato, M. Tamai, T. Isshiki, K. Nishio, H. Aritani, Synthesis of nanotube from a layered $H_2Ti_4O_9{\cdot}H_2O$ in a hydrothermal treatment using various titania sources, J. Mater. Sci. 39 (2004) 4239–4245.
[15] A. Kukovecz, M. Hodos, E. Horváth, G. Radnóczi, Z. Kenya, I. Kiricsi, Oriented crystal growth model explains the formation of titania nanotubes, J. Phys. Chem. B 109 (2005) 17781–17783.
[16] C. Dames, B. Poudel, W. Wang, J. Huang, Z. Ren, Y. Sun, J. Oh, C. Opeil, M.J. Naughton, G. Chen, Low-dimensional phonon specific heat of titanium dioxide nanotubes, Appl. Phys. Lett. 87 (2005) 031901.
[17] D. Bavykin, J. Friedrich, A. Lapkin, F. Walsh, Stability of aqueous suspensions of titanate nanotubes, Chem. Mater. 18 (2006) 1124–1129.
[18] E. Morgado, M.S. de Abreu, O. Pravia, B. Marinkovic, P. Jardim, F. Rizzo, A. Araujo, A study on the structure and thermal stability of titanate nanotubes as a function of sodium content, Solid State Sci. 8 (2006) 888–900.
[19] L. Qian, Z. Du, S. Yang, Z. Jin, Raman study of titania nanotube by soft chemical process, J. Mol. Struct. 749 (2005) 103–107.
[20] H. Xu, G. Vanamu, Z. Nie, H. Konishi, R. Yeredla, J. Phillips, Y. Wang, Photocatalytic oxidation of a volatile organic component of acetaldehyde using titanium oxide nanotubes, J. Nanomaterials (2006) 78902.

[21] M. Adachi, Y. Murata, I. Okada, S. Yoshikawa, Formation of titania nanotubes and applications for dye-sensitized solar cells, J. Electrochem. Soc. 150 (2003) G488.
[22] D. Bavykin, A. Lapkin, P. Plucinski, J. Friedrich, F. Walsh, Reversible storage of molecular hydrogen by sorption into multilayered TiO_2 nanotubes, J. Phys. Chem. B 109 (2005) 19422.
[23] M. Hodos, Z. Kónya, G. Tasi, I. Kiricsi, Catalysis by pre-prepared platinum nanoparticles supported on trititanate nanotubes, React. Kinet. Catal. Lett. 84 (2005) 341–350.
[24] C. Tsai, H. Teng, Regulation of the physical characteristics of titania nanotube aggregates synthesized from hydrothermal treatment, Chem. Mater. 16 (2004) 4352–4358.
[25] M. Cortés-Jácome, G. Ferrat-Torres, L.F. Flores Ortiz, C. Ángeles Chávez, E. López-Salinas, J. Escobar, M.L. Mosqueira, J.A. Toledo-Antonio, In situ termo-Raman study of titanium oxide nanotubes, Catal. Today 126 (2007) 248–255.
[26] M. Cortés-Jácome, J. Escobar, C. Ángeles Chávez, E. López-Salinas, E. Romero, G. Ferrat, J. Toledo-Antonio, Highly dispersed CoMoS phase on titania nanotubes as efficient HDS catalysts, Catal. Today 130 (2008) 56–62.
[27] J.A. Toledo-Antonio, M.A. Cortés-Jácome, C. Angeles-Chávez, J. Escobar, M.C. Barrera, E. López-Salinas, Highly active CoMoS phase on titania nanotubes as new hydrodesulfurization catalysts, Appl. Catal. B 90 (2009) 213–223.
[28] M.A. Khan, O.-B. Yang, Photocatalytic water splitting for hydrogen production under visible light on Ir and Co ionized titania nanotube, Catal. Today 146 (2009) 177–182.
[29] K. Nishijima, Y. Fujisawa, N. Murakami, T. Tsubota, T. Ohno, Development of an S-doped titania nanotube (TNT) site-selectively loaded with iron (III) oxide and its photocatalytic activities, Appl. Catal. B 84 (2008) 584–590.
[30] V. Idakiev, Z. Yuan, T. Tabakova, B. Su, Titanium oxide nanotubes as supports of nano-sized gold catalysts for low temperature water-gas shift reaction, Appl. Catal. A 281 (2005) 149–155.
[31] S.V. Awate, R.K. Sahu, M.D. Kadgaonkar, R. Kumar, N.M. Gupta, Photocatalytic mineralization of benzene over gold containing titania nanotubes: role of adsorbed water and nanosize gold crystallites, Catal. Today 141 (2009) 144–151.
[32] L.C. Sikuvhihulu, N.J. Coville, T. Ntho, M.S. Scurrell, Potassium titanate: an alternative support for gold catalyzed carbon monoxide oxidation? Catal. Lett. 123 (2008) 193–197.
[33] T.A. Ntho, J.A. Anderson, M.S. Scurrell, CO oxidation over titanate nanotube supported Au: deactivation due to bicarbonate, J. Catal. 261 (2009) 94–100.
[34] Y. Suzuki, S. Yoshikawa, Synthesis and thermal analysis of TiO_2-derived nanotubes prepared by the hydrothermal method, J. Mater. Res. 19 (2004) 982–985.
[35] M. Haruta, T. Kobayashi, H. Sano, N. Yamada, Novel gold catalysts for the oxidation of carbon monoxide at a temperature far below 0 °C, Chem. Lett. (1987) 405–408.
[36] M. Haruta, Size- and support-dependency in the catalysis of gold, Catal. Today 36 (1997) 153–166.
[37] M. Haruta, M. Daté, Advances in the catalysis of Au nanoparticles, Appl. Catal. A 222 (2001) 427–437.
[38] R. Zanella, S. Giorgio, C. Henry, C. Louis, Alternative methods for the preparation of gold nanoparticles supported on TiO_2, J. Phys. Chem. B 106 (2002) 7634–7642.
[39] R. Zanella, S. Giorgio, C.H. Shin, C.R. Henry, C. Louis, Characterization and reactivity in CO oxidation of gold nanoparticles supported on TiO_2 prepared by deposition-precipitation with NaOH and urea, J. Catal. 222 (2004) 357–367.
[40] R. Zanella, L. Delannoy, C. Louis, Mechanism of deposition of gold precursors onto TiO_2 during the preparation by cation adsorption and deposition–precipitation with NaOH and urea, Appl. Catal. A 291 (2005) 62–72.
[41] R. Zanella, C. Louis, Influence of the conditions of thermal treatments and of storage on the size of the gold particles in Au/TiO_2 samples, Catal. Today 107–108 (2005) 768–777.
[42] G.C. Bond, Gold: a relatively new catalyst, Gold Bull. 34 (2001) 117.